River ice and water velocities using the Planet optical cubesat constellation

Andreas Kääb[1], Bas Altena[1], Joseph Mascaro[2]

[1]Department of Geosciences, University of Oslo, Oslo, 0316, Norway
5 [2]Planet, San Francisco, postal code 94103, USA

Correspondence to: Andreas Kääb (kaeaeb@geo.uio.no)

Abstract. The PlanetScope constellation consists of ~150 optical cubesats that are evenly distributed like strings of pearls in two orbital planes and scan the Earth's land surface once per day with ~3m spatial image resolution. Subsequent cubesats in each of the orbital planes image the Earth surface with a nominal time lapse of ~90s between each other, which produces

10 near-simultaneous pairs of scenes over the across-track overlaps of the cubesat swaths. We exploit this short time lapse between subsequent Planet cubesat images to track river ice floes on Northern rivers as indicators of water surface velocities. The method is demonstrated for a 60km long reach of the Amur River in Siberia, and a 200km long reach of the Yukon River, Alaska. The accuracy of the estimated horizontal surface velocities is on the order of ±0.01 m s^{-1}. The application of our approach is complicated by cloud cover and low sun angles at high latitudes during the periods where rivers typically

15 carry ice floes, and by the fact that the near-simultaneous swath overlaps by design do not cover the complete Earth surface. Still, the approach enables direct remote sensing of river surface velocities over many cold-region rivers and several times per year — much more frequent and over much larger areas than feasible so far, if at all. We find that freeze-up conditions seem in general to offer ice floes that are more suitable for tracking, and over longer time periods, compared to typical ice break-up conditions. The coverage of river velocities obtained could be particularly useful in combination with satellite

20 measurements of river area, and river surface height and slope.

1 Introduction

Knowledge about water-surface velocities on rivers supports understanding a wide range of processes. In cold regions, river-ice freeze-up and in particular break-up, and the associated transport of and action by ice debris is often the most important hydrological event of the year, producing flood levels typically exceeding those for other periods (Fig. 1) and with dramatic

25 consequences for river ecology and infrastructure (e.g., Prowse et al., 2007; Kääb and Prowse, 2011; Rokaya et al., 2018a). River discharge measurements are complicated during freeze-up and break-up due to the physical impact of ice on instrumentation, and determination of water surface speeds from tracking river ice floes can contribute to estimate discharge (Beltaos and Kääb, 2014). This possibility is of particular importance for the major Arctic rivers of North America and

Siberia, which transport large amounts of freshwater into the Arctic ocean, but the discharge of which is least known for the time of ice break-up – notably the time where annual discharge peaks (Zakharova et al., 2019).

During periods where rivers carry ice floes, or other visible surface objects, water velocities can be measured using near-simultaneous satellite (or airborne) images, optimally with time separations on the order of minutes (Kääb and Leprince, 2014). Such near-simultaneous imaging of the Earth surface is provided by satellite stereo sensors, where the two or more stereo image partners are by necessity temporally separated by ~1-2 minutes (Kääb and Leprince, 2014). Ice floes (or other floating objects) are then tracked over this time lapse to estimate water surface velocities during the time of image acquisition. Satellite stereo imaging that is useful for this purpose stems either from fixed stereo or agile stereo. (In principle, also satellite video could be used to track ice floes but has to our best knowledge not been demonstrated yet for this purpose; (d'Angelo et al., 2014; d'Angelo et al., 2016)). Fixed stereo is provided by two or more fixed cameras with different along-track viewing angles; e.g., the ASTER or ALOS PRISM sensors; agile stereo is provided by one single camera that is rotated during overflight to point repeatedly to the same ground target; e.g., WorldView or Pleiades satellites. Kääb and Prowse (2011) demonstrated the method deriving river ice and water velocities over short reaches of the Mackenzie and St. Lawrence Rivers, Canada, using both types of satellite stereo images. Kääb et al. (2013) used ASTER fixed satellite stereo to measure and analyse river ice flux and water velocities over a 600km long reach of Lena River, Siberia. Finally, Beltaos and Kääb (2014) demonstrated how such-derived water surface velocity fields can be used to estimate river discharge. Even if Kääb and Leprince (2014) indicate other seasons and satellite constellations to track river ice floes over short time spans, all the above studies have in common that they (i) use for the most part images during ice break-up, (ii) use dedicated stereo systems, and (iii) use mostly rare and opportunistic acquisitions. Point (i) limits application of the method to one short time period of the year, and (ii) and in particular (iii) prevent from applying the method operationally and systematically over large reaches of many rivers. The PlanetScope cubesat constellation, however, offers a new possibility to perform such systematic worldwide observations of river ice velocities and water velocities indicated by them. The primary aim of the current study is to demonstrate and explore these possibilities, and a second aim is to evaluate estimation of water velocities during river freeze-up, instead of during break-up.

The PlanetScope optical cubesat constellation scans the Earth surface systematically and daily (Figs. 1 and 2) involving overlap of consecutive acquisitions with a time-lag of around 1.5 minutes. Such order of time-lag is perfectly suited to track floating matter, in particular river-ice floes. PlanetScope offers thus the possibility for systematic daily measurement of water surface velocities, as long as ice floes are present on the water and sky conditions are clear. In this study, we first introduce in more detail the PlanetScope cubesat constellation. After a short description of the methods used to track ice floes over minute-scale time lags, we demonstrate and discuss typical ice-floe conditions suitable for tracking, and derived velocities over a 60km long reach of Amur River, Siberia, and a 200km long reach of Yukon River, Alaska. We also discuss the error budget of the measurements in detail. Finally, we draw conclusions on the potential for systematically measuring river ice and water velocities from the PlanetScope constellation and shortly sketch out possible application fields.
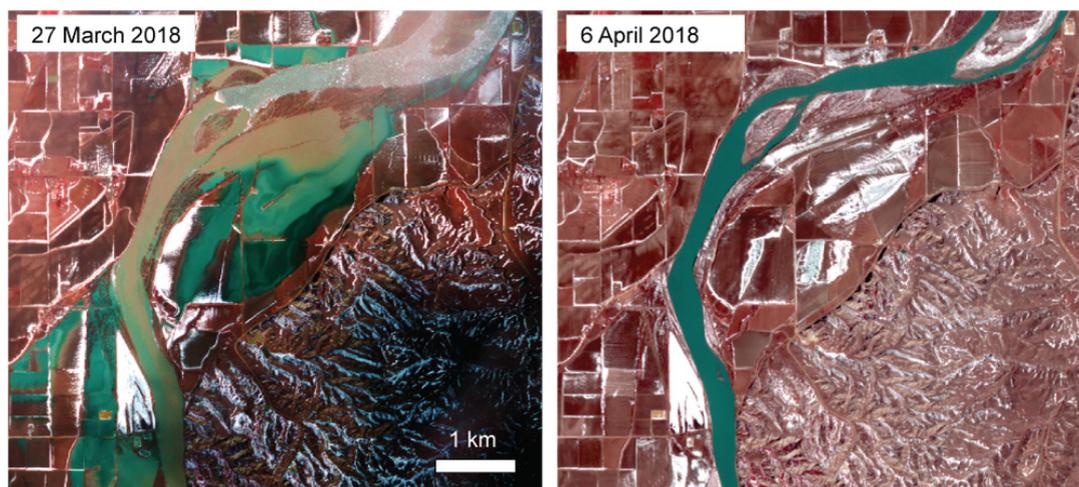
Figure 1: Planet images over an ice jam on Yellowstone River at Sidney, NE, USA (47.75° N, 104.09° W). The river flows from bottom to top (North). Left: ice jam (top) and associated flooding. Right: break of the ice jam.

5 2 The Planet cubesat constellation

The following descriptions of the Planet constellation and data, and the methods used, are an update and specification of the descriptions given by Kääb et al. (2017). (Text in "quotation marks" is only slightly updated from the latter reference.) "The Planet cubesat constellation, called PlanetScope or more popular 'Doves', have a size of about 10 cm × 10 cm × 30 cm, making them 3-unit (3U) cubesats. Their main component is a telescope and CCD area array sensor, complemented by solar

10 panels for power generation, a GNSS receiver for satellite position, a star-tracker for satellite orientation, reaction wheels for attitude control and stabilisation, an antenna for down- and uplink, batteries and on-board storage. One half of the 6600 × 4400 pixel CCD array acquires red-green-blue (RGB) data and the other half near-infrared (NIR), both in 12 bit radiometric resolution. The PlanetScope satellites provide images of about 3.7 m spatial resolution at an altitude of 475 km (delivered as resampled to 3 m), and a size of individual scenes of roughly 25-30 km × 8-10 km (Planet Team, 2019). Ground resolution

15 and scene size vary slightly with flying height and satellite version. While most other optical Earth observation instruments in space deliver images in pushbroom geometry (i.e. linear sensor arrays scanning the swath width in orbit direction), the data from the Planet satellites are frame images, so far mostly known for airborne or ground sensors. That is, each complete scene is taken at one single point in time, has one single acquisition position and one single bundle of projection rays. For comparison, pushbroom sensors integrate an image over a certain time interval so that acquisition time, position and attitude

20 angles vary throughout an image, which may lead to higher-order image distortions (Nuth and Kääb, 2011; Kääb et al., 2013; Girod et al., 2015) ."

"The Planet cubesat constellation consists currently of around 150 cubesats following each other in two near-polar orbits of ~8° and ~98° inclination, respectively, and an altitude of ~475 km (Fig. 2), imaging the Earth at local morning from both an ascending and descending orbit. The distance of the cubesats to each other in each orbit is designed in a way so that the longitudinal progression between them over the rotating Earth leads to a void-less scan of the surface (except the polar hole)

5 and the full constellation provides sun-synchronous coverage of the entire Earth with daily temporal resolution (Fig. 2)(Foster et al., 2015)." (Kääb et al., 2017). To guarantee this void-less surface imaging at all latitudes and also during times when satellite positions and pointing angles are not exactly nominal, the swaths of subsequent cubesats overlap in across-track direction by some kilometres (Figs. 2 and 3). Within these swath-overlaps Earth surface targets are imaged twice (rarely also more) with a time lag of very roughly 1.5 minutes. It is this time lag that we exploit in the current study. The

10 PlanetScope constellation involves also other time lags (e.g., < 1s between RGB and NIR acquisitions; a few hours, depending on latitude, between acquisitions from ascending and descending orbits) that are however not the focus here.

During the PlanetScope constellation's technological demonstration phase the cubesats were mostly launched from the International Space Station into an orbit of 52° inclination and ~375 km height (Fig. 2)(Kääb et al., 2017). Data from these satellites form the majority of Planet's cubesat data archive holding for 2016 and into early 2017, before acquisitions from

15 the near-polar sun-synchronous orbits took over.
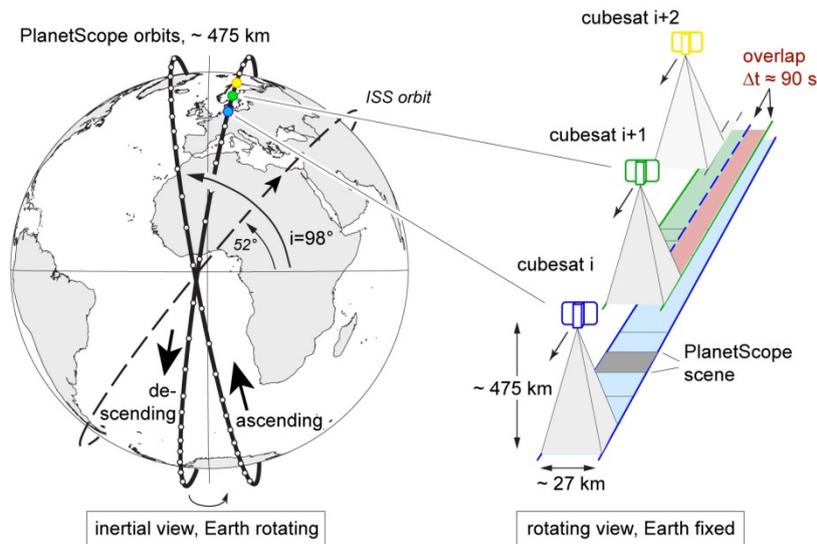
Figure 2: Planet orbits. Left, inertial view: final PlanetScope descending and ascending orbits (bold) and ISS test-bed orbit (dashed). Cubesat positions (white dots on the orbits) are only schematically indicated. Right, rotating view: scheme of complete
20 **scan of the Earth surface by successive PlanetScope cubesats (called doves) in the same orbit producing a time lapse of around 90 seconds over the swath overlaps.**
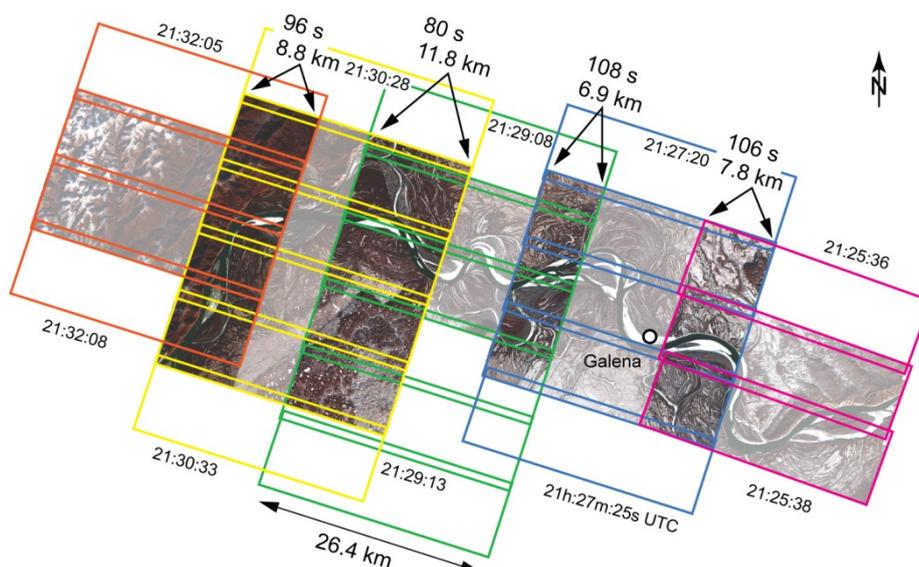
Figure 3: Typical PlanetScope acquisition pattern on a cloud-free day during freeze-up (28 October 2018) over the Yukon River at Galena, Alaska (64.75° N, 157° W). Each colour indicates one satellite swath with individual scenes. Non-dimmed image parts indicate scene sections where two images with time lapse between them exist and river ice floes can be tracked. Time lapse and width of the overlaps are given together with UTC time of the acquisitions.

3 Data and methods

Within the swath overlaps and over the corresponding ~1.5 min time lapse we track river ice floes using image matching techniques. "For image matching purposes the geometric characteristics of repeat imagery is of particular interest. PlanetScope images are available in different processing levels, and here we use 'analytic' data. 'Analytic' data are radiometrically processed and orthorectified. The examples in this study do not apply 'unrectified' data, another processing level available, which comes with minimal radiometric processing and in the original frame geometry, i.e. central projection. The image orientation parameters from on-board measurements are refined by Planet by matching the scenes onto a global reference mosaic (currently from Landsat, ALOS and Open Street Map layers) and the images are orthoprojected using a DEM. As for all orthoprojected satellite data, vertical errors in the orthorectification DEM lead to lateral distortions in the resulting PlanetScope orthoimages, the size of which is proportional to the DEM error and the off-nadir viewing angle (Kääb et al., 2016; Altena and Kaab, 2017)." (Kääb et al., 2017). For a worst-case scenario for PlanetScope data (Kääb et al., 2017) a DEM error of 10 m results in an orthorectification offsets of around 30 cm in the scene centre and 65 cm at the outer scene margin. For repeat river observations the differential effect of these offsets can be reduced by co-registering the near-simultaneous (~1.5 min) images using stable points along shorelines. Over the limited width of rivers, water surface topography is approximately planar, which makes a first-order co-registration model strictly sufficient to bring repeat

'unrectified' frame images into overlap, but this procedure will also greatly reduced offsets between the orthorectified 'analytic' images used here as the same DEM is used for both near-simultaneous images (Kääb et al., 2017). Errors in the DEMs used for orthorectifying PlanetScope images are a composite of DEM elevation errors with respect to the real topography at the time of DEM acquisition, and of real-world elevation changes between elevations at DEM acquisition and

5   elevations at satellite image acquisition. Orthorectification DEMs are by necessity outdated (though generally with limited consequences) unless acquired simultaneously with image acquisition. For river surfaces, the latter elevation deviations will primarily stem from water-level variations between DEM and image acquisition dates. "The small field of view of PlanetScope cubesats and the resulting small sensitivity to topographic distortions, the frame geometry of the PlanetScope cameras, and the accessibility of unrectified images, if needed, all contribute to minimize and potentially remove

10   topographic distortions."

"For matching the repeat PlanetScope data we use standard normalized cross-correlation (NCC), solving the cross-correlation in the spatial domain and reaching sub-pixel accuracy by interpolation of the image (Kääb and Vollmer, 2000; Debella-Gilo and Kääb, 2011a; Kääb, 2014). The matching window sizes used for the PlanetScope data are 30×30 pixels (90×90 m) as found roughly optimal from a few tests. Tests with different window sizes are, though, not the focus of this

15   study (Debella-Gilo and Kääb, 2011b). Measurements with a correlation coefficient smaller 0.7 are removed and no other post-processing is applied." (Kääb et al., 2017).

4 Results

4.1 River ice conditions

Figure 4 illustrates a small subset of typical river ice conditions in Planet images that are suitable for tracking ice floes or ice

20   features, and estimate water velocities. During break-up we find predominantly smaller ice floes with very variable densities of ice-floe cover (Fig. 4, right column). During freeze-up we find typically bigger ice floes and a more equal distribution of ice-floe cover density over the river surface. Clearly, this simple description of differences between freeze-up and break-up ice conditions is an overall and qualitative one based on a substantial, though, visual exploration of Planet archive holdings, but a range of exceptions and natural variations certainly exist. Our Planet image archive research suggests clearly that

25   during freeze-up ice conditions suitable for tracking are more constant over time and stretch over longer time periods (up to several days or even a week, roughly) compared to break-up conditions. Break-up ice conditions suitable for tracking last typically only one or several ice pulses of a few days in maximum, often just a day or two. This makes the capture of suitable ice conditions during freeze-up less sensitive to cloud cover than during break-up. On the other hand, the freeze-up period reaches at the northernmost latitudes into the season of low sun angle, where Planet cubesats (and other optical satellite

30   instruments) do not acquire data. Still, the clear overall impression from our archive research is that it is typically easier to find Planet images suitable for tracking ice floes over freeze-up than over break-up periods.
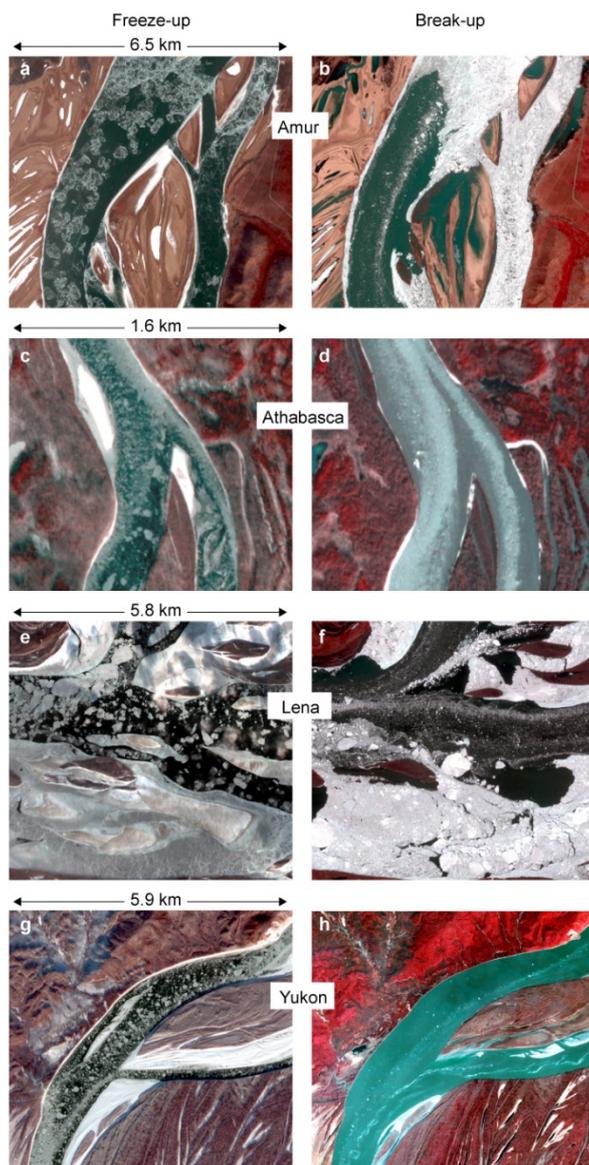
Figure 4: Typical river ice conditions in Planet imagery (shown in infrared false colour) that is suitable for tracking ice floes to estimate water velocities. Left column: during freeze-up; right column: during break-up.

4.1 Amur River, Siberia

For a first example of river ice velocities from near-simultaneous Planet cubesat images we mosaic two overlapping sets of 12 scenes each into two image strips covering a ~60km long reach of the Amur River near the city of Komsomolsk-on-Amur, eastern Siberia. The image-strip pair was acquired on 1 November 2016 (~22:46 UTC) from an International Space

5   Station (ISS) orbit, with a 73 s time lapse. Figure 5a shows one of the two image strips as an infrared false colour composite. The freeze-up river ice conditions during the acquisition were close to perfect for matching velocities; ice floes densely covered most of the water surface, but were at the same time for most areas not juxtaposed so that ice floe velocities should to a large extent indicate water velocities. Figure 5b shows the magnitudes of the velocities derived, with maximum speeds of 1.7 m s^{-1} close to the lower end of the river reach investigated. Successful displacements on the floodplain surrounding the

10   river are sparse as the surface seems to consist mostly of homogenous shrubs that offer little visual contrast to match at the image resolution of 3m. The images used in this example stem from an early generation of Planet cubesats with reduced contrast compared to current sensors. In addition, contrast is reduced by the low sun angle during acquisition. The latter two complications, however, have little adverse effect on the matches of ice floes as these offer strong and little sensitive contrast against the surrounding dark water surface. Figure 6 shows a detail (rectangle in Fig. 5) of the original velocity vectors

15   measured. Grid spacing of the vectors is 75m.
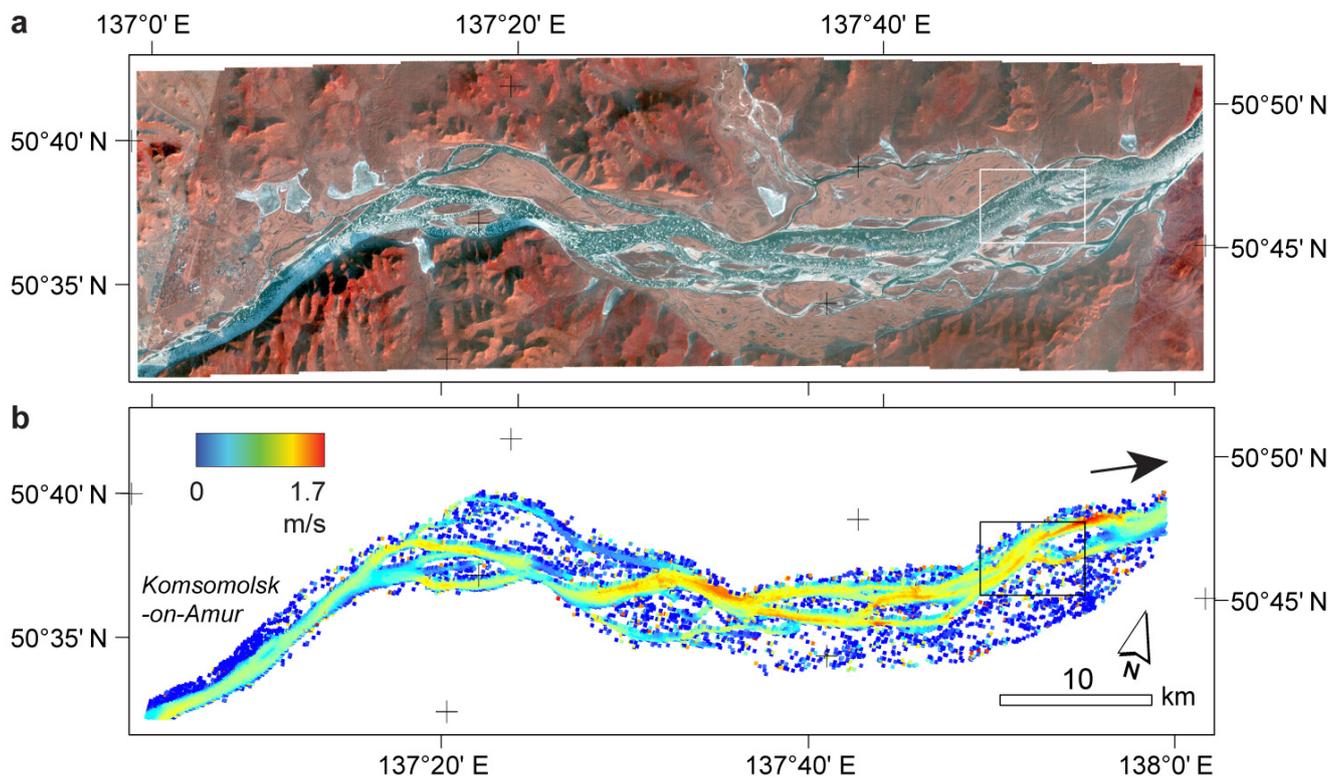
Figure 5: Amur River near the city of Komsomolsk-on-Amur, Siberia (lower left corner). River surface velocities of 1 November 2016 are tracked over a 73s time lapse between overlapping Planet cubesat images. (a) False colour composite of one of the image strips. (b) Derived surface speeds. Flow direction to the right. The small rectangle marks the location of detail Fig. 5.
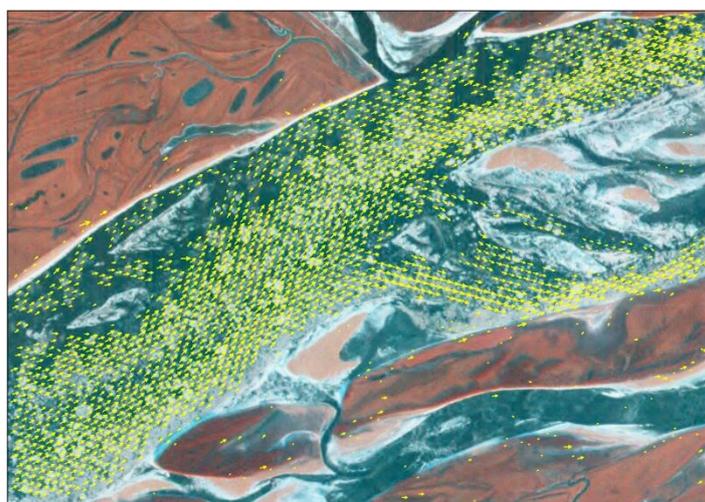
Figure 6: Detail of Fig. 5 (small rectangle). Original matched surface velocities after thresholding of the correlation coefficient. Grid spacing of vectors is 75m. Maximum speed 1.7 m s^{-1}.

4.2 Yukon River, Alaska

For a second case study we choose a ~200 km long reach of the Yukon River, Alaska (Fig. 7). Over this reach, the overall river azimuth coincides with the azimuth of the near-polar descending orbit of the Planet cubesats. We mosaic sequences of around 25 scenes each to obtain two image strips for 16 May 2017 (~21:12 UTC) with 15s time lapse, and two images strips for 4 November 2018 (~21:30 UTC) with 171s time lapse. Typical ice conditions for these acquisitions are demonstrated in Figs. 4h and g, respectively. The velocity magnitudes derived are shown in Figs. 7 c and e, speed differences between them in Fig. 7d, and a detail of these three items in Fig. 8. For comparison, we add river ice speeds derived for 13 May 2014 from a strip of ASTER stereo pairs (i.e. 55s time lapse) following the method by Kääb et al. (2013) and compute differences to the 16 May 2017 Planet data set (Figs 7 a and b). On 13 May 2014, river ice cover was comparably sparse and subsequently also the successful velocity matches. The freeze-up conditions of 4 November 2018 clearly offered the most complete cover by river ice floes and thus the most complete velocity field. The river outlines used in Figs. 7 and 8 were obtained as a raster-to-vector conversion of a noise-filtered and thresholded band ratio image between the blue and thermal infrared bands of Landsat scenes of 16 September 2013. Visually, these outlines represent the actual outlines of May 2014 and May 2017 very well, without significant changes over time. At shallow river parts, outlines of November 2018 (i.e. low water conditions) were of course more narrow than for September 2013. The outlines produced here are however only used for visualisation, and initial result segmentation into classes "river" and "outside river" for accuracy assessment on stable ground.

The closest river discharge measurements to our Yukon River reach are done at Pilot Station (no. 15565447), some 300km downstream of the lower end of the reach studied. For 13 May 2014 and 16 May 2017 discharge estimates at Pilot Station are 11,383 m^3 s^{-1} and 8,410 m^3 s^{-1}, respectively. At the time of writing values for 4 November 2018 were not yet available, but the average of the years 2014-2017 for this day of the year is 5,324 m^3 s^{-1}. Taking into account the distance between the reach investigated and Pilot Station, we also give the discharges 3 days later: 13,450 m^3 s^{-1}, 11,213 m^3 s^{-1}, 4,927 m^3 s^{-1} for 16 May 2014, 19 May 2017, and 7 November 2018. As for the discharges also the surface velocities measured for 13 May 2014 are higher than for 16 May 2017, and the latter ones are higher than for 4 November 2018.

Although not exploited closer in this study, we would like to note the existence of a Sentinel-2 scene of 4 November 2018, taken about one hour after the Planet scenes. Due to this large time lapse between the Planet and Sentinel-2 scenes and the related large displacements and deformations/rotations of river ice features, traditional image matching methods are complicated, but manual tracking of distinct floes is still clearly possible. Tests show good agreement between the speeds derived over 1h and those over 171s. The fact that most Planet cubesats, Sentinel-2A and 2B, and Landsat7 and 8 are on similar orbits can thus create additional opportunities for tracking river ice movement, for investigating short-term changes in river ice cover and speed, and for additional, or combined, multispectral mapping and analysis with respect to the Planet cubesats.

Figure 9a shows the longitudinal profile of speeds for the 4 November 2018 data set, together with the river width automatically derived from the velocity vectors. Further we also compute the 2-dimensional (2D) surface flux as a function of transverse velocity profiles. As an example for interpretation of the longitudinal profile, at ~80km 2D surface flux is relatively low, suggesting under mass conservation that the Yukon River should be relatively deep at this part of the reach. In

5   contrast, the river should be on average relatively shallow at, for instance, ~120km.

From a similar profile of river surface speed along 400km of the Lena River during 27 May 2011, Kääb et al. (2013) found a striking peak in the power spectrum of river surface speed at 20.8km. For the Yukon River profile Fig. 9 we find a somewhat less prominent but still significant peak in the power spectrum of speeds at 20.5km. The similar number for both river reaches might point to similar processes and parameters for the development of the respective river morphologies (Lanzoni,

10   2000a, b).

Profile Fig. 9b compares river surface speeds and river widths of 16 May 2017 and 4 November 2018. The four data sets are consistent in the sense of mass conservation; higher discharges in May 2017 compared to November 2018 (see above discharges for Pilot Station) correspond to a combination of larger widths and higher surface speeds. For instance, at sections where river width is significantly larger in May 2017 than November 2018, speed differences between May 2017 and

15   November 2018 are smaller (e.g. at ~60, 110 or 170km). Conversely, at sections with relatively small changes in river width, surface speeds change more (e.g. at ~30, 90, or 130km).
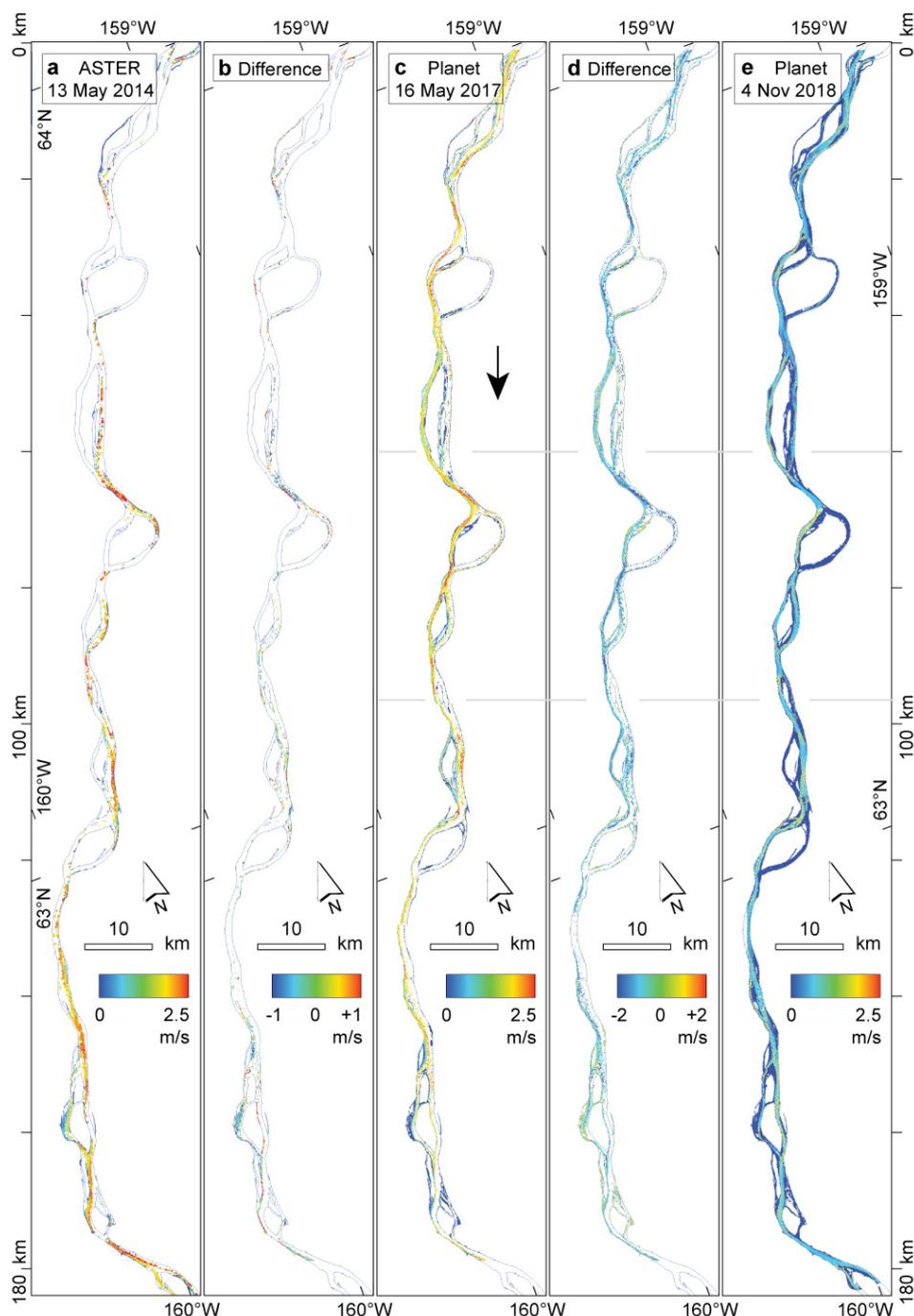
Figure 7: Surface velocities on Yukon River, Alaska, from near-simultaneous satellite images. Flow direction roughly from north to south, top to bottom of figure. Velocities from (a) an ASTER stereo pair of 13 May 2014 (55s time lapse), (c) two Planet cubesat image strips of 16 May 2017 (15s), and (e) of two Planet cubesat image strips of 4 November 2018 (171s). Panels (b) and (d) show
5 **the differences (c)-(a) and (e)-(c), respectively. The horizontal grey lines in panels (c) to (e) indicate the detail shown in Fig. 8.**
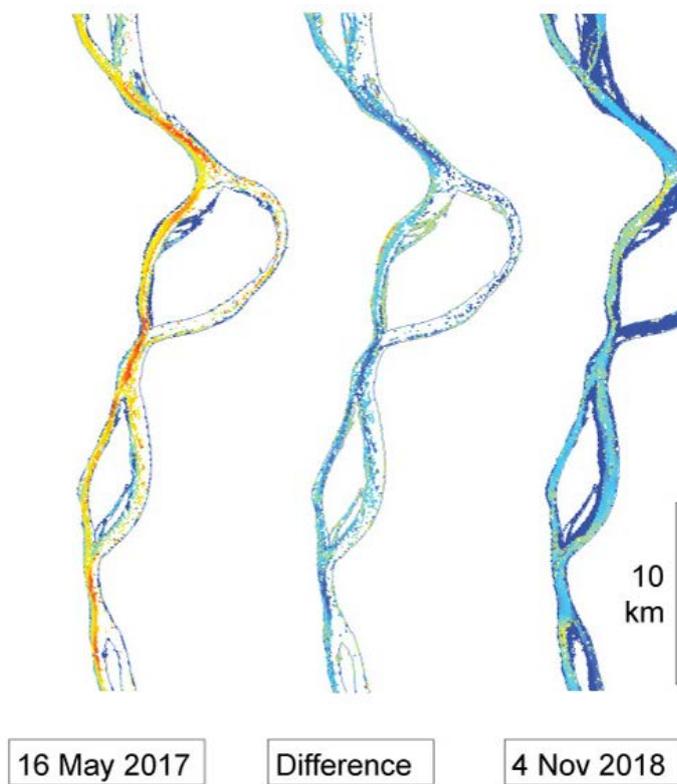
Figure 8: Detail of Fig. 7. For more information see caption of Fig. 7.
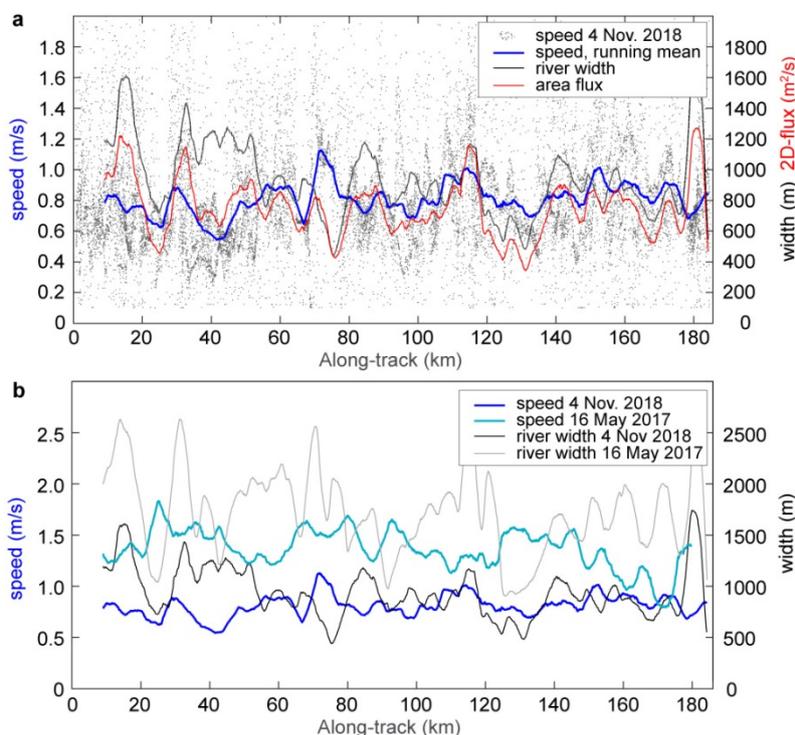
Figure 9: Longitudinal profile of speeds and river widths derived from near-simultaneous Planet cubesat images. (a) Measurements of 4 November 2018. Small dots: individual speed measurements; blue line: 4km running mean of individual measurements; black line: river width from velocities (running mean); red line: surface area flux as product of cross-sectional average speed and river width (running mean). (b) Running means of surface speeds and river width for 4 November 2018 (dark blue and black, respectively) and 16 May 2017 (light blue and grey, respectively).

4.3 Error budget

The error budget for individual river surface velocity measurements consists of three main components: (i) absolute georeference of a set of repeat images, (ii) relative distortions and offsets between repeat images, and (iii) errors from matching features between the repeat images. The first category, the uncertainty of the absolute georeference, stems mostly from matching the Planet images onto a reference image. This step is part of the Planet in-house processing and is to our experience typically on the order of one pixel or less, but can be larger for partially cloud-covered or for snow-covered scenes. Failure or gross uncertainties of this georeference refinement step and subsequent gross georeference errors are flagged by Planet in the image meta-data. To our best knowledge, an absolute georeference accuracy of a few meters or pixels for the locations of derived velocities should not be a problem for most applications, in particular when considering that the derived velocities anyway represent a window of several tens of metres (here 90m × 90m). The second category of

uncertainty, (ii), distortions and offsets between the images matched, can be minimized by co-registration, which is typically possible with sub-pixel accuracy. This uncertainty source is not necessary completely eliminated for small-scale higher-order distortions (see section on Data and Methods) that differ between the stable ground used for co-registration (river shore, flood plain, etc.) and the actual river surface. The parts of this second error component that are not eliminated by image co-registration, mix with the third error category, that is the actual matching accuracy for the stable ground or river ice features (iii). This relative matching accuracy between already co-registered images defines the actual uncertainty of the actual displacements or velocities derived, and we thus consider it here as the error component of largest interest (Kääb et al., 2013) and focus on it in more detail in the following.

Uncertainties of individual velocity measurements or outliers (our above error component iii) stem from uncertainties in definition of river-ice features over time, i.e. how sharp can features be matched that change over time and how (precisely) is a displacement between slightly modified features defined. This error component includes the representativeness of displacements matched using a 90m × 90m window for actual point-wise velocities, and the degradation of the matching accuracy by rotation or deformation of river-ice features over the minute-scale time lapse exploited (Kääb et al., 2013). We estimate the accuracy of our river ice velocity measurements in three ways: (1) inferring from previous studies, (2) stable ground matches, and (3) variance of velocities within homogenous parts of the derived flow field. (1) Based on ASTER data over the Lena river, Kääb et al. (2013) suggest for most optimal imaging and ice conditions an displacement accuracy of up to 1/8 of a pixel, which would in our case translate to about $\pm$ 0.4 – 0.5 m (or 0.005 m s^{-1} for a 90s time lapse). (2) Based on about 27'000 matches on the floodplains around the rivers investigated in this study we obtain a mean displacement dx of -0.1 $\pm$ 0.5 m, dy of -0.2 $\pm$ 0.6 m, and mean displacement length (Pythagoras of individual dx and dy) of 0.6 $\pm$ 0.6 m. Besides a good co-registration accuracy of around 0.2 m (i.e. about 1/15 of a pixel), our stable ground tests suggest thus an accuracy of individual velocity measurements of $\pm$0.6 m (1/5 of a pixel; 0.007 m s^{-1}). This latter number agrees well with the accuracy estimates for coseismic displacement measurements from repeat Planet data of 1/4 of a pixel (Kääb et al., 2017). Finally, (3), variations of velocities within homogenous parts of the derived flow fields, i.e. the standard deviation of means over such parts of the flow fields, range in our tests between $\pm$0.3m for the shortest time lapse in our study (15s; translating to 0.02 m s^{-1}) and $\pm$3m for our longest time lapse (171s; 0.02 m s^{-1}). Especially for the longer time lapses, deformations of the rive ice features matched and rotations of individual ice floes certainly degrade the actual matching accuracy. From all our above three approaches we suggest thus as a rule of thumb an accuracy on the order of $\pm$0.01 m s^{-1} for individual river ice velocities derived from near-simultaneous PlanetScope data. Note that this accuracy improves following standard error propagation rules, once individual velocities are averaged, for instance for cross-sectional or longitudinal means.

5 Discussion, conclusions, and outlook

In this study we exploit the fact that the cross-track overlaps of the swaths of subsequent PlanetScope cubesats (Figs. 2 and 3) produce near-simultaneous optical acquisitions, separated by ~90s. Over this time lapse we track river ice floes and use them as indicator for water surface velocities. Planet cubesats scan the entire land surface of the Earth at daily repeat and

5   with ~3m spatial image resolution. Our study shows that these data substantially extend the possibilities to measure river ice and water surface flow from near-simultaneous optical satellite data. Over many rivers that carry river ice, ice floes can be tracked several times per year during freeze-up and/or break-up with accuracies on the order of ±0.01 m s^{-1}. Freeze-up conditions appear to be particularly well suited for this work due to the longer time periods and more favourable types and densities of ice floes present.

10   We find three main obstacles when applying the method. By constellation design the PlanetScope cross-track overlaps (never intended for measuring minute-scale changes and motions) cover not the entire Earth surface but only parts of it, depending on latitude, for instance 2/3 of a cubesat swath for 65° North (Fig. 3). Second, cloud cover seems not untypical for the river freeze-up and break-up seasons, and complicates the acquisition of suitable Planet cubesat data — as for any optical satellite instrument. Third, freeze-up for some northern-most rivers or river reaches seems to happen during sun angles that

15   are too low to acquire suitable images. Despite these three main limitations, though, the tracking of river ice in near-simultaneous Planet cubesat data substantially increases the possibilities for deriving surface velocities on cold-region rivers.

Such data can complement other methods of velocity measurements, namely radar interferometry (Romeiser et al., 2007). As demonstrated here for a 200km long reach of the Yukon River, remotely sensed water velocities over long reaches might offer improved insights in river morphology. For instance, we find a variation of water speeds of ~20-21 km wavelength for

20   the Yukon River (and the Lena River; Kääb et al. (2013)) that could be compared to according wavelengths found from laboratory experiments and models on bar formation (Lanzoni, 2000a, b).

A major purpose of satellite observations of rivers are attempts to estimate discharge in order to spatially or temporally complement the sparse in-situ measurements available from gauging stations (Beltaos and Kääb, 2014; Bjerklie et al., 2018; Zakharova et al., 2019; and many others, see references in the cited ones). River velocities from the approach demonstrated

25   here can offer an additional type of input measurement, or a possibility for independent comparison/validation, when linking satellite-based measurements of river height and slope from altimetry data, and measurement of river surface from optical (Allen and Pavelsky, 2018) or radar images, to standard discharge equations (Bjerklie et al., 2018; Zakharova et al., 2019). Such satellite data are available over large regions (Allen and Pavelsky, 2018) and fit thus well to the river velocities as derived by our approach. Satellite-altimetric river heights will even improve in the (near) future through the new ICESat-2

30   and upcoming SWOT missions, and Landsat 8 and Sentinel-2 together offer sub-weekly repeat to measure actual river surface parameters.

As further outlook, the water mapping opportunities from the daily repeat Planet data (Cooley et al., 2017) together with opportunities to measure ice velocities from them as demonstrated here could aid detecting ice jams and related flooding (Cooley et al., 2017)(Fig. 1), and better understanding of the mechanisms involved in ice jam formation. The damages from ice jam floods cause annual economic costs on the order of several hundred millions EUR per year in North America and

5   Siberia (Prowse et al., 2007; Rokaya et al., 2018b, a). Finally, while substantially fewer in number, we speculate that near-simultaneous overpasses in tropical and temperate rivers could similarly be exploited, tracking sediment or floating matter in place of ice (Kääb and Leprince, 2014).

Code availability

The image matching code used for this study (Correlation Image AnalysiS, CIAS) is available from
10   http://www.mn.uio.no/icemass.

Data availability

Sentinel-2 data are freely available from the ESA/EC Copernicus Sentinels Scientific Data Hub at https://scihub.copernicus.eu/ , Landsat 8 data from USGS at http://earthexplorer.usgs.gov/ , ASTER data from https://earthdata.nasa.gov/ , Yukon River discharge data from https://waterdata.usgs.gov. Planet data are not openly available
15   as Planet is a commercial company. However, scientific access schemes to these data exist.

Author contribution

A.K. developed the study, did most of the analyses and wrote the paper. B.A. supported the analyses and edited the paper. J.M. helped with data acquisition, technical details to the Planet constellation and data, and edited the paper.

Competing interests

20   A.K. and B.A. declare that they have no competing interests. J.M. is program manager for impact initiatives at Planet. He did in no manner influence the results or conclusions of the study.

Acknowledgements

We are grateful to the providers of data for this study; Planet for their cubesat data via Planet's Ambassadors Program, ESA/Copernicus for Sentinel-2 data, USGS for Landsat 8 and river discharge data, and NASA and the ASTER science team
25   at JPL for ASTER data. Special thanks are due to Michael Abrams for tasking the May 2014 ASTER acquisitions over the

Yukon River. The work was funded by the European Research Council under the European Union's Seventh Framework Programme (FP/2007-2013) / ERC grant agreement no. 320816, the ESA project Glaciers_cci (4000109873/14/I-NB), the ESA Living Planet Fellowship to B.A. (4000125560/18/I-NS), and the ESA EarthExplorer10 Mission Advisory Group.

References

Allen, G. H., and Pavelsky, T. M.: Global extent of rivers and streams, Science, 361, 585-587, doi 10.1126/science.aat0636, 2018.

Altena, B., and Kääb, A.: Elevation Change and Improved Velocity Retrieval Using Orthorectified Optical Satellite Data from Different Orbits, Remote Sens-Basel, 9, ARTN 300, doi 10.3390/rs9030300, 2017.

Beltaos, S., and Kääb, A.: Estimating river discharge during ice breakup from near-simultaneous satellite imagery, Cold Reg Sci Technol, 98, 35-46, doi 10.1016/j.coldregions.2013.10.010, 2014.

Bjerklie, D. M., Birkett, C. M., Jones, J. W., Carabajal, C., Rover, J. A., Fulton, J. W., and Garambois, P. A.: Satellite remote sensing estimation of river discharge: Application to the Yukon River Alaska, J Hydrol, 561, 1000-1018, doi 10.1016/j.jhydrol.2018.04.005, 2018.

Cooley, S. W., Smith, L. C., Stepan, L., and Mascaro, J.: Tracking Dynamic Northern Surface Water Changes with High-Frequency Planet CubeSat Imagery, Remote Sens-Basel, 9, ARTN 1306, doi 10.3390/rs9121306, 2017.

d'Angelo, P., Kuschk, G., and Reinartz, P.: Evaluation of Skybox Video and Still Image Products, Int Arch Photogramm, 40-1, 95-99, doi 10.5194/isprsarchives-XL-1-95-2014, 2014.

d'Angelo, P., Mattyus, G., and Reinartz, P.: Skybox image and video product evaluation, Int J Image Data Fus, 7, 3-18, doi 10.1080/19479832.2015.1109565, 2016.

Debella-Gilo, M., and Kääb, A.: Sub-pixel precision image matching for measuring surface displacements on mass movements using normalized cross-correlation, Remote Sens Environ, 115, 130-142, doi 10.1016/j.rse.2010.08.012, 2011a.

Debella-Gilo, M., and Kääb, A.: Locally adaptive template sizes in matching repeat images of Earth surface mass movements, ISPRS J Photogramm, 69, 10-28, doi 10.1016/j.rse.2010.08.012, 2011b.

Foster, C., Hallam, H., and Mason, J.: Orbit determination and differential-drag control of Planet Labs cubesat constellation, AIAA Astrodynamics Specialist Conference in Vale, CO, August 2015, https://arxiv.org/pdf/1509.03270v03271.pdf, 2015

Girod, L., Nuth, C., and Kääb, A.: Improvement of DEM generation from ASTER images using satellite jitter estimation and open source implementation The International Archives of the Photogrammetry, Remote Sensing and Spatial Information Sciences, XL-1/W5, 2015.

Kääb, A., and Vollmer, M.: Surface geometry, thickness changes and flow fields on creeping mountain permafrost: automatic extraction by digital image analysis, Permafrost Periglac 11, 315-326, doi 10.1002/1099-1530(200012)11:4<315::Aid-Ppp365>3.0.Co;2-J, 2000.

Kääb, A., and Prowse, T.: Cold-regions river flow observed from space, Geophys Res Lett, 38, L08403, 2011.

Kääb, A., Lamare, M., and Abrams, M.: River ice flux and water velocities along a 600 km-long reach of Lena River, Siberia, from satellite stereo, Hydrol Earth Syst Sc, 17, 4671-4683, doi 10.5194/hess-17-4671-2013, 2013.

Kääb, A.: Correlation Image Analysis software (CIAS), http://www.mn.uio.no/icemass, last visited 5.2.2019, 2014.

Kääb, A., and Leprince, S.: Motion detection using near-simultaneous satellite acquisitions, 154, 164-179, doi 10.1016/j.rse.2014.08.015, 2014.

Kääb, A., Winsvold, S. H., Altena, B., Nuth, C., Nagler, T., and Wuite, J.: Glacier remote sensing using Sentinel-2. Part I: radiometric and geometric performance, and application to ice velocity, Remote Sens., 8, 598, doi 10.3390/Rs8070598, 2016.

Kääb, A., Altena, B., and Mascaro, J.: Coseismic displacements of the 14 November 2016 Mw 7.8 Kaikoura, New Zealand, earthquake using the Planet optical cubesat constellation, Nat Hazard Earth Sys, 17, 627-639, doi 10.5194/nhess-17-627-2017. 2017.

Lanzoni, S.: Experiments on bar formation in a straight flume 1. Uniform sediment, Water Resour Res, 36, 3337-3349, doi 10.1029/2000wr900160, 2000a.

Lanzoni, S.: Experiments on bar formation in a straight flume 2. Graded sediment, Water Resour Res, 36, 3351-3363, doi 10.1029/2000wr900161, 2000b.

Nuth, C., and Kääb, A.: Co-registration and bias corrections of satellite elevation data sets for quantifying glacier thickness change, Cryosphere, 5, 271-290, doi 10.5194/tc-5-271-2011, 2011.

Planet Application Program Interface: In Space for Life on Earth. San Francisco, CA. https//api.planet.com/ and https//www.planet.com/. last visited 01.01.2019., 2019.

Prowse, T. D., Bonsal, B., Duguay, C. R., Hessen, D. O., and Vuglinsky, V. S.: River and lake ice, in: Global Outlook for Ice & Snow, United Nations Environment Programme, 201-214, 2007.

Rokaya, P., Budhathoki, S., and Lindenschmidt, K. E.: Trends in the Timing and Magnitude of Ice-Jam Floods in Canada, Sci Rep-Uk, 8, ARTN 5834, doi 10.1038/s41598-018-24057-z, 2018a.

Rokaya, P., Budhathoki, S., and Lindenschmidt, K. E.: Ice-jam flood research: a scoping review, Nat Hazards, 94, 1439-1457, doi 10.1007/s11069-018-3455-0, 2018b.

Romeiser, R., Runge, H., Suchandt, S., Sprenger, J., Weilbeer, H., Sohrmann, A., and Stammer, D.: Current measurements in rivers by spaceborne along-track InSAR, IEEE T Geosci Remote, 45, 4019-4031, doi 10.1109/Tgrs.2007.904837, 2007.

Zakharova, E. A., Krylenko, I. N., and Kouraev, A. V.: Use of non-polar orbiting satellite radar altimeters of the Jason series for estimation of river input to the Arctic Ocean, J Hydrol, 568, 322-333, doi 10.1016/j.jhydrol.2018.10.068, 2019.